Am J Transl Res 2024;16(12):7396-7404
www.ajtr.org /ISSN:1943-8141/AJTR0159912

Original Article

Value of CT diagnostic techniques based on imaging post-processing systems in the early diagnosis and treatment of lung cancer

Wanling Li[1], Xuelan Zheng[2], Jishui Huang[3]

[1]*Computed Magnetic Resonance Imaging Tomography, The Second Affiliated Hospital of Fujian Medical University, Quanzhou 362000, Fujian, China;* [2]*Intensive Care Unit, The Second Affiliated Hospital of Fujian Medical University, Quanzhou 362000, Fujian, China;* [3]*Respiratory and Critical Care Medicine, Nan'an City Hospital, Quanzhou 362399, Fujian, China*

Received August 19, 2024; Accepted November 26, 2024; Epub December 15, 2024; Published December 30, 2024

Abstract: Objective: To evaluate the application value of CT diagnostic technology based on the Shukun Imaging Post-Processing System for early screening and diagnosis of lung cancer. Methods: A total of 35 patients diagnosed with lung cancer postoperatively and 53 patients with benign nodules were included in this retrospective study, all of whom were treated in the Department of Thoracic and Cardiovascular Surgery of the Second Affiliated Hospital of Fujian Medical University from January 2020 to December 2023. All patients underwent chest spiral CT examinations. Original thin-slice axial CT images were processed using Shukun software for three-dimensional reconstruction of the lesions, surrounding lung tissue, and trachea. The diagnoses and malignant risk indicators of pulmonary nodules were established based on the final imaging results. Results: Statistical analysis showed that the sensitivity of Shukun processing technology in diagnosing early-stage lung cancer was 82.86%, with a specificity of 88.46%, when compared to postoperative pathological analysis. Univariate logistic regression analysis indicated that features such as burr sign, lobulation sign, pleural traction sign, vascular convergence sign, vacuole sign, and nodule size derived from Shukun processing had significant predictive value for malignant nodules ($P<0.05$). Conclusion: Shukun processing technology can effectively reconstruct ordinary CT tomographic images into three-dimensional representations, enhancing the visualization of spatial relationships between the tumor and adjacent anatomical structures, including trachea, pleura, bronchi, and blood vessels. It has high clinical diagnostic value for the early diagnosis of malignant pulmonary nodules.

Keywords: Pulmonary nodule, chest CT, Shukun imaging post-processing system, lung cancer, diagnostic efficacy

Introduction

A pulmonary nodule is defined as a solid lung lesion measuring less than 3 cm in diameter [1, 2]. These small nodules are often incidentally identified through chest X-rays or high-resolution CT scans. Their characteristics can vary, including benign, malignant, or atypical hyperplasia, which represents an intermediate state between the two [3, 4]. Benign pulmonary nodules may originate from infections, inflammations, or other non-neoplastic conditions, while malignant nodules typically indicate precancerous or early-stage lung cancer, with treatment and prognosis closely linked to the timely detection. The relationship between pulmonary nodules and lung cancer is intricate; not all pulmonary nodules progress to lung cancer [5, 6].

Statistical evidence indicates that pulmonary nodules smaller than 5 mm have a very low probability of developing into lung cancer, whereas the risk of malignancy increases with nodule size [7, 8]. Currently, the primary imaging modality for lung cancer diagnosis is spiral CT. However, conventional axial CT images often fail to provide accurate qualitative assessments of lung tissue lesions, resulting in a low rate of early lung cancer diagnosis. Shukun Imaging Post-Processing software enhances standard CT scans by reconstructing images into three-dimensional representations, there-

https://doi.org/10.62347/VJSR2965

by clarifying the anatomy of pulmonary nodules, surrounding tissues, and blood vessels, which may improve the detection rate of malignant tumors [9, 10]. Based on this background, this study aims to evaluate the diagnostic efficacy of this technology in 88 patients with pulmonary nodules, contributing to enhanced approaches for diagnosing malignant lung tumors.

Materials and methods

Patient selection

Between January 2022 and June 2023, a total of 35 patients with lung cancer and 53 patients with benign nodules were admitted to the Department of Thoracic and Cardiovascular Surgery at the Second Affiliated Hospital of Fujian Medical University.

This retrospective study aimed to estimate the sample size for two groups in a parallel 1:1 design, dividing patients into a malignant group and a benign group. Based on previous comparisons of diagnostic effects using similar image post-processing systems for pulmonary nodules, the average diagnostic coincidence rates were μ1 = 0.8 for the control group and μ2 = 0.9 for the observation group, with a standard deviation of s = 0.1. Accounting for a 10% dropout rate and setting the type I error rate (α) at 0.05 with a confidence level of (1-β) = 80%, the required sample size was calculated using the formula:

$$n1 = n2 = \frac{2(Za/2 + Z\beta)^2 \times \sigma^2}{(\mu 1 - \mu 2)^2}$$

Substituting the values (μ1 = 0.8, μ2 = 0.9, σ = 1, α = 0.05, β = 0.2), the calculations yielded n1 = n2 = 12, leading to a minimum sample size of 24. To enhance the reliability of the results, all eligible patients during the study period, totaling 88 cases, were included.

Inclusion criteria

1. Preoperative chest CT indicating nodules with a diameter greater than 8 mm; 2. Presence of common imaging features of nodules, including spiculation, calcification, satellite lesions, pleural traction sign, lobulation sign, and vascular sign; 3. Availability of complete standard medical records, including current and past history, as well as comprehensive preoperative laboratory and imaging examination results; 4. Completion of chest and related examinations at our hospital.

Exclusion criteria

1. Patients with concurrent liver, lung, or gastrointestinal tumors identified during preoperative examinations; 2. Patients exhibiting multiple nodules in both lungs on chest CT, where pathology cannot be determined; 3. Patients with well-defined pulmonary masses suspected to be advanced tumors with associated thrombosis or compression; 4. Patients experiencing significant organ dysfunction, such as heart or kidney failure; 5. Patients with mental illness or speech disorders that impede normal communication; 6. Patients with incomplete clinical data.

Data acquisition

Data were obtained by reviewing the electronic medical record system, including patient blood test results and CT scan images. The chest CT examinations were conducted using a 64-slice spiral CT scanner with the following parameters: tube voltage of 120 kV, tube current of 300 mA, pitch of 1.375:1, scan layer thickness of 5.0 mm, matrix of 512×512, and reconstruction layer thickness of 1.25 mm. A comprehensive lung scan was performed for all patients based on the above parameters. After the examination, the images were uploaded to a central workstation, where the Shukun Imaging Post-Processing System performed three-dimensional reconstructions. Imaging diagnostic specialists then reviewed the reconstructed images to identify relevant pulmonary tissues. The system automatically generated parameters related to the lesions, including size, shape, and location. A preliminary diagnostic assessment for the lesion was subsequently formulated based on these imaging characteristics.

Observation indicators

Primary observation indicators: The final diagnostic criteria for lung cancer, which included pathological examination of lung lesions, evaluation of tissue morphology, and staining and immunohistochemical analysis to determine the pathological classification of lung nodules, were employed to compare the sensitivity, specificity, positive predictive value, negative predictive value, and accuracy of the automatic

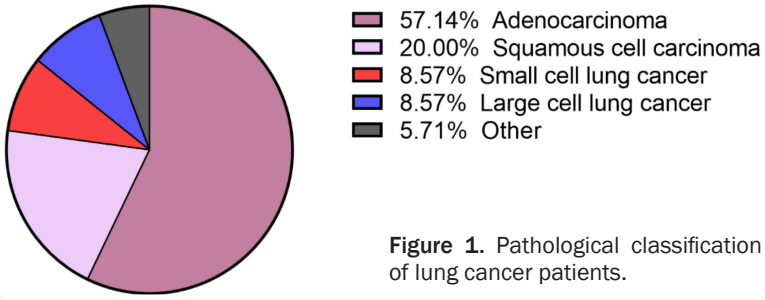

Figure 1. Pathological classification of lung cancer patients.

Table 1. The diagnostic efficiency of lung nodule Shukun processing software

		CT/Shukun System		Total
		Malignant	Benign	
Pathological examination results	Malignant	29	6	35
	Benign	7	46	53
	Total	36	52	88

diagnostic results generated by the Shukun processing software, thereby evaluating its diagnostic efficacy. Additionally, the predictive capacity of various imaging characteristics of pulmonary nodules for distinguishing between benign and malignant outcomes was assessed [11].

Secondary observation indicators: Comparisons were made of peripheral blood test results between the benign and malignant groups, including routine blood tests, liver and kidney function assessments, and lung cancer markers, to explore the efficacy of hematological indicators in diagnosing malignant lung tumors.

Data analysis

Data analysis was performed using SPSS 22.0 software. Measurement data were expressed as mean ± SEM. The t-test was used for analyzing measurement data with a normal distribution. Paired sample t-tests were employed for within-group comparisons, while independent sample t-tests were applied for between-group comparisons. For data that did not follow a normal distribution, the Mann-Whitney U test was used. Count data were expressed as rates (percentages) and analyzed using the x^2 test. Variables with statistically significant differences in univariate analysis were included in logistic regression analysis to calculate the odds ratio (OR) and its 95% confidence interval (CI). A *P*-value of less than 0.05 was considered statistically significant.

Results

Final pathological reports of the 88 cases

Among the 88 cases examined, 35 patients (39.78%) were pathologically diagnosed with lung cancer, while 53 patients (60.22%) were diagnosed with non-lung cancer conditions. The types and composition of lung cancer cases are shown in **Figure 1**.

Automatic diagnostic results of pulmonary nodules using Shukun processing software

The analysis of the CT/Shukun system processing technology revealed a sensitivity of 82.86%, a specificity of 88.46%, a positive predictive value of 80.56%, and a negative predictive value of 86.80% for early-stage lung cancer diagnosis, indicating a relatively high diagnostic value for this technology. The area under the curve (AUC) was 0.848, with a 95% CI of 0.758 to 0.938 (**Table 1** and **Figure 2**). Typical images processed using the CT/Shukun system are shown in **Figure 3**.

Comparison of baseline data between malignant and benign groups

No statistically significant differences were found in gender, age, and BMI between the two groups, indicating comparability (**Table 2**).

Comparison of serological data between malignant and benign groups

Similarly, the comparison of serological data indicated no statistically significant differences in gender, age, and BMI between the two groups, indicating comparability (**Table 3**).

Comparison of serum tumor marker levels between malignant and benign groups

Analysis of serum tumor markers revealed no statistically significant differences in peripheral blood levels of carcinoembryonic antigen (CEA), neuron-specific enolase (NSE), and cytokeratin fragment 19 (CYFRA21-1) (P = 0.773, 0.666 and 0.720, respectively) (**Figure 4**).

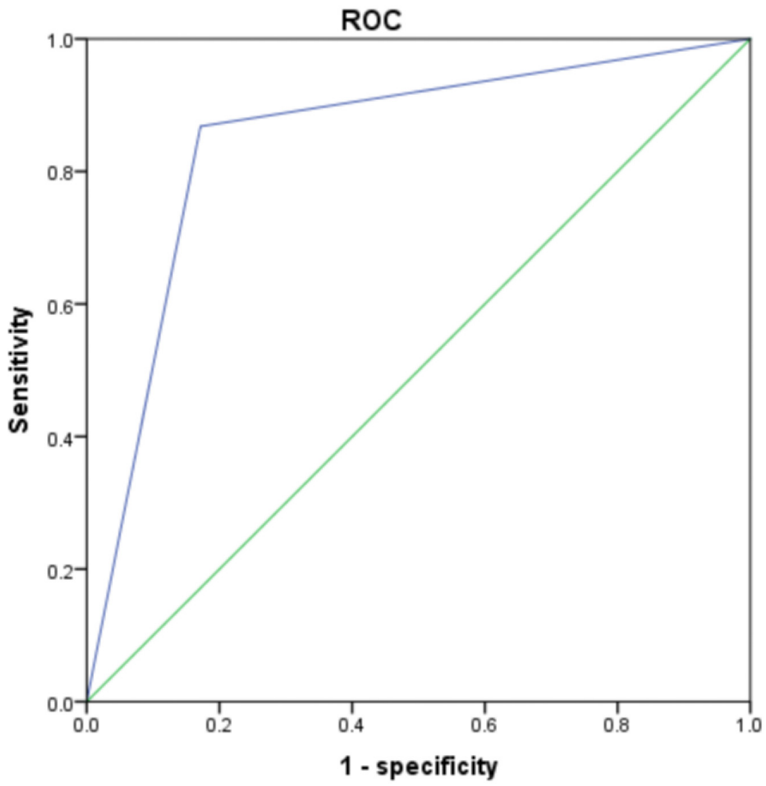

Figure 2. The AUC diagram of the diagnosis of pulmonary nodules by Shukun system.

Differences in imaging features between malignant and benign groups

Statistically significant differences were observed between the malignant and benign groups in terms of spiculation, lobulation, pleural traction sign, vascular convergence sign, vacuole sign, size, calcification, and satellite lesions. Multivariate analysis identified these factors as independent influencing factors for the malignancy of pulmonary nodules (**Tables 4**, **5** and **Figures 5**, **6**).

Discussion

Pulmonary nodules generally refer to small, round or oval lesions within the lung parenchyma, typically measuring less than 3 cm in diameter. When a pulmonary nodule exceeds this threshold, it is classified as a pulmonary mass [12]. The nature of these nodules can be benign or malignant; benign nodules may arise from inflammation, infection, or benign tumors, whereas malignant nodules are usually associated with lung cancer [13-15]. Therefore, the early diagnosis of the nature of pulmonary nodules is crucial for improving patient prognosis. Epidemiological studies show that the detection rate of pulmonary nodules has significantly increased with the widespread use of high-resolution CT (HRCT). Among populations undergoing chest CT scans, the proportion of detected pulmonary nodules can exceed 50% [16-18].

Since its introduction in the 1970s, CT scanning technology has undergone revolutionary advancements in the medical field. Compared to traditional X-ray examinations, CT provides more detailed and clearer images of internal structures, particularly in complex organs like the lungs. By utilizing a high-speed rotating X-ray emitter and receiver, CT scans can capture images from different angles, which are then processed by computer algorithms to reconstruct three-dimensional, well-defined images. This technology allows doctors to observe the lung's overall structure and accurately locate, measure, and analyze the characteristics of pulmonary nodules, making it the preferred method for lung examinations [19, 20]. However, conventional axial CT images often fail to provide effective qualitative diagnoses of lung tissue lesions, leading to lower rates of early lung cancer detection [21, 22]. In contrast, the Shukun Imaging Post-Processing System enhances conventional CT scans by reconstructing and processing images to present pulmonary nodules and surrounding tissues and blood vessels in a three-dimensional anatomical format. This advancement improves the detection rate of malignant lung tumors.

Previous studies have demonstrated that image post-processing systems can significantly enhance the diagnostic accuracy of malignant pulmonary nodules. The Shukun system employs innovative three-dimensional reconstruction technology based on standard spiral CT scans, distinguishing it from other CT post-processing techniques such as MPR, MIP, and

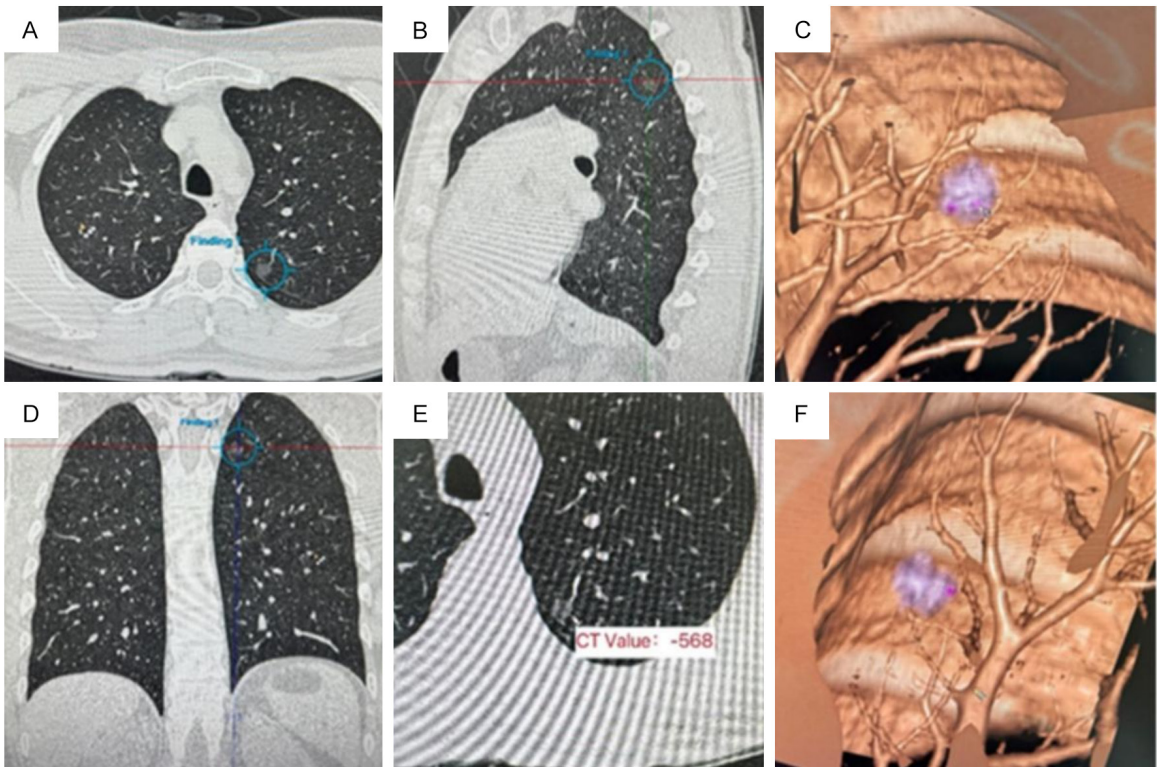

Figure 3. Classic image of lung nodules. Three-dimensional reconstruction of pulmonary nodules using CT plain scan and Shukun post-processing technology. Panels (A) and (D) show the horizontal view of the left lower pulmonary nodule, panels (B) and (E) display the coronal view, and panels (C) and (F) present the three-dimensional reconstruction of the lung nodule generated by the post-processing system.

Table 2. Comparison of baseline data between the two groups

Group	Gender (Male/Female)	Age	BMI	Hypertension	Nodule Distribution (Left/Right)	Time of Nodule Detection
Malignant group (n = 35)	20/15	37.8±5.2	23.2±2.7	7	18/17	2.8±0.4
Benign group (n = 53)	30/23	38.0±5.9	24.1±2.8	5	29/24	2.5±0.5
Statistical value	0.002	-0.163	-1.497	1.202	0.092	-0.992
P	0.960	0.871	0.138	0.273	0.762	0.324

Table 3. Comparison of serum related examinations between the two groups

Group	WBC ($\times 10^9$)	AST (U/L)	ALT (U/L)	Scr (mmol/L)	NEU ($\times 10^9$)	LYM ($\times 10^9$)
Malignant group (n = 35)	9.88±1.2	20.5±2.4	22.6±2.7	71.6±4.8	5.45±2.25	1.39±0.62
Benign group (n = 53)	9.65±1.4	22.2±2.8	21.9±2.9	72.0±5.0	5.37±2.16	1.32±0.43
Statistical value	0.797	-1.213	1.139	-0.373	0.167	0.626
P	0.428	0.228	0.258	0.710	0.868	0.533

CRP. Myrian software, for example, plays a critical role in clinical screening, diagnosis, disease assessment, and surgical guidance. By offering three-dimensional reconstructions, it provides a more intuitive and comprehensive view of the anatomical structures of lesions, adjacent tissues, and blood vessels. This capability not only increases the early detection rate of tumors but also offers valuable guidance for surgical intervention [23]. In our study, the Shukun Imaging Post-Processing System was used to diagnose 88 patients with pulmonary nodules. Pathological confirmation revealed that 35 patients had lung cancer, while 55 had

Table 4. Univariate analysis of malignant transformation in patients with pulmonary nodules

CT Findings	Benign group (n = 53)	Malignant group (n = 35)	F/χ^2	*P*
Spiculation	13	19	8.066	0.005
Lobulation	16	19	5.110	0.024
Pleural traction sign	11	17	7.518	0.006
Vascular convergence sign	12	16	5.173	0.023
Vacuole sign	8	15	8.416	0.004
Nodule size				
>1 cm	44	20	7.396	0.006
≤1 cm	9	15		
Calcification	16	22	9.170	0.002
Satellite lesions	10	18	10.302	0.001

Table 5. Logistic analysis of pulmonary nodule malignancy

Variable	Standardized β	OR	95% CI	P
Spiculation	0.884	3.46	1.47-8.89	0.038
Lobulation	0.747	3.21	1.36-7.26	0.032
Pleural traction sign	0.558	4.27	1.15-7.48	0.020
Vascular convergence sign	0.487	4.42	1.26-8.15	0.002
Vacuole sign	0.665	3.73	1.17-9.13	0.024
Nodule size >1 cm	0.849	3.71	1.05-8.66	0.005
Calcification	-3.023	0.49	0.32-0.64	0.047
Satellite lesions	-4.328	0.85	0.44-0.77	0.004

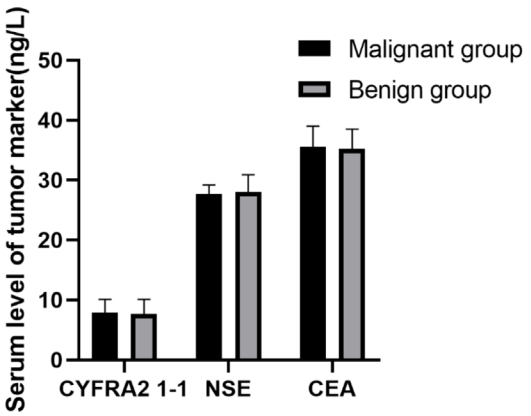

Figure 4. Comparison of serum tumor markers CEA, NSE, and CYFRA21-1 between the two groups. Note: CEA: carcinoembryonic antigen, NSE: neuron-specific enolase; CYFRA21-1: cytokeratin fragment 19.

benign lesions. Statistical analysis showed that the Shukun Post-Processing System achieved a sensitivity of 82.86%, specificity of 88.46%, positive predictive value of 80.56%, and negative predictive value of 86.80%. The AUC was 0.848, with a 95% CI of 0.758 to 0.938, indicating that the Shukun Imaging Post-Processing System possesses good diagnostic value for lung cancer. These findings are consistent with results reported in previous studies [23, 24].

In addition, previous imaging studies have demonstrated that various imaging features can aid in differentiating between benign and malignant tumors, including the burr sign, lobulation sign, pleural traction sign, vascular convergence sign, and vacuole sign, which are commonly associated with malignancies. Conversely, calcification is typically indicative of benign lesions [25]. Our analysis of imaging data revealed statistically significant differences between benign and malignant pulmonary nodules in terms of spiculation, lobulation, pleural traction sign, vascular convergence sign, vacuole sign, size, calcification, and satellite lesions. Logistic regression analysis indicated that these characteristics serve as independent imaging factors for the malignancy of pulmonary nodules, whereas calcification and satellite lesions were identified as protective factors. The underlying mechanisms for these imaging characteristics are as follows: Spiculation occurs due to tumor cell infiltration into adjacent bronchovascular sheaths or local

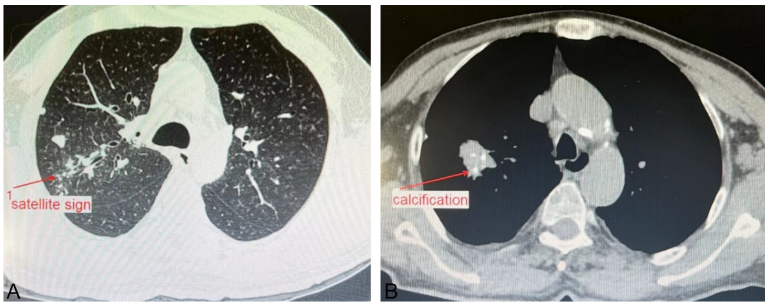

Figure 5. Satellite focus and calcification of pulmonary nodules. A: Pulmonary nodules satellite focus; B: Calcification image.

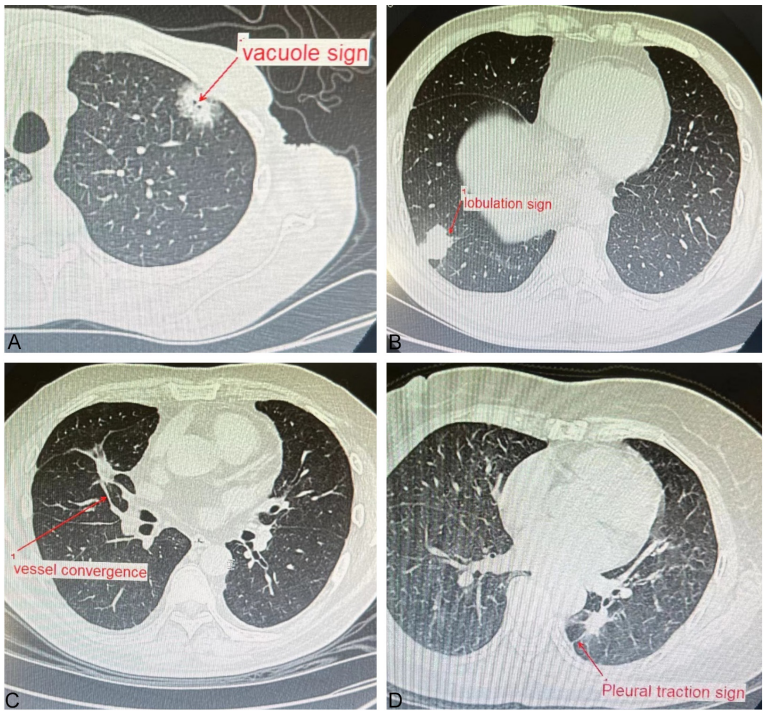

Figure 6. Images of pulmonary nodular lobulation sign, pleural traction sign, vascular convergence sign and vacuole sign. A: Vacuole sign; B: Lobulation sign; C: Vascular convergence sign; D: Pleural traction sign.

lymphatics, or as a result of the stimulation of connective tissue formation by tumor-associated fibrous bands. Radiographically, this manifests as short, radiating, unbranched lines extending from the edge of the lung mass or nodule into the surrounding parenchyma, without connecting to the pleura. Lobulation is primarily due to the uniform density of peripheral lung cancer. The pleural traction sign occurs when nodules exert a pulling effect on the pleura, while the vascular convergence sign is mainly characterized by thickened vascular structures, reflecting the increased blood supply needed for rapidly growing nodules. The vacuole sign manifests as 1-3 mm low-density areas within the nodule due to residual air-containing lung tissue or bronchi. The size of the pulmonary nodule correlates directly with the likelihood of malignancy. Studies have reported that nodules with a maximum diameter of 1 cm are more likely to be malignant, as malignant nodules generally exhibit more rapid growth than benign ones. Our study also showed that calcification and satellite lesions are protective factors against the malignancy of pulmonary nodules. Calcification in pulmonary nodules is commonly seen in post-inflammatory nodules, such as those resulting from tuberculosis or pulmonary hamartomas, which are often benign. Satellite lesions, smaller nodules located near the primary nodule, resemble satellites around the primary nodule and are typically indicative of benign conditions. These findings are consistent with the conclusions of previous researchers [25, 26].

Previous studies have demonstrated that serological markers in patients diagnosed with early-stage lung cancer often exhibit no significant abnormalities [27]. In our study, we further explored the correlation between serological markers and malignant lung tumors. Our results showed no statistically significant differences in peripheral blood routine tests and tumor markers, including CEA, NSE, and CYFRA21-1, between the two groups. This finding is consistent with previous conclusions regarding the limited diagnostic efficacy of serological markers for lung cancer, aligning with current clinical practices where serum markers are not widely used for early screening of lung cancer [27, 28]. However, some studies still suggest that tumor markers, such as CEA, NSE, and CYFRA21-1, possess significant predictive value, likely associated

with larger tumor sizes and more advanced stages of the patients in these studies. Therefore, effective serum tumor markers could potentially play an important role in the diagnosis, treatment, and prognosis of lung cancer.

In conclusion, the Shukun Imaging Post-Processing System, through three-dimensional reconstruction of standard CT images of the lungs, demonstrates good diagnostic value for lung cancer. However, this study has the following limitations: certain findings require further validation through larger sample sizes in subsequent studies, and improving the efficacy of serological markers in lung cancer diagnosis remains a crucial area for future research to strengthen the conclusions of this research.

Disclosure of conflict of interest

None.

Address correspondence to: Jishui Huang, Respiratory and Critical Care Medicine, Nan'an City Hospital, No. 2330, Jiangbei Avenue, Liucheng Street, Quanzhou 362399, Fujian, China. Tel: +86-13055621788; E-mail: 15860432790@163.com

References

[1] Mazzone PJ and Lam L. Evaluating the patient with a pulmonary nodule: a review. JAMA 2022; 327: 264-273.

[2] Khodayari Moez E, Warkentin MT, Brhane Y, Lam S, Field JK, Liu G, Zulueta JJ, Valencia K, Mesa-Guzman M, Nialet AP, Atkar-Khattra S, Davies MPA, Grant B, Murison K, Montuenga LM, Amos CI, Robbins HA, Johansson M and Hung RJ. Circulating proteome for pulmonary nodule malignancy. J Natl Cancer Inst 2023; 115: 1060-1070.

[3] Astaraki M, Zakko Y, Toma Dasu I, Smedby Ö and Wang C. Benign-malignant pulmonary nodule classification in low-dose CT with convolutional features. Phys Med 2021; 83: 146-153.

[4] Sears CR and Mazzone PJ. Biomarkers in lung cancer. Clin Chest Med 2020; 41: 115-127.

[5] Wu Z, Wang F, Cao W, Qin C, Dong X, Yang Z, Zheng Y, Luo Z, Zhao L, Yu Y, Xu Y, Li J, Tang W, Shen S, Wu N, Tan F, Li N and He J. Lung cancer risk prediction models based on pulmonary nodules: a systematic review. Thorac Cancer 2022; 13: 664-677.

[6] de Margerie-Mellon C and Chassagnon G. Artificial intelligence: a critical review of applications for lung nodule and lung cancer. Diagn Interv Imaging 2023; 104: 11-17.

[7] Ogan N, Baha A, Özan Sanhal E, Alhan A and Gülhan M. Incidental pulmonary nodule frequency in Turkey. Tuberk Toraks 2019; 67: 190-196.

[8] Chilet-Rosell E, Parker LA, Hernández-Aguado I, Pastor-Valero M, Vilar J, González-Álvarez I, Salinas-Serrano JM, Lorente-Fernández F, Domingo ML and Lumbreras B. The determinants of lung cancer after detecting a solitary pulmonary nodule are different in men and women, for both chest radiograph and CT. PLoS One 2019; 14: e0221134.

[9] Wang B, Si S, Zhao H, Zhu H and Dou S. False positive reduction in pulmonary nodule classification using 3D texture and edge feature in CT images. Technol Health Care 2021; 29: 1071-1088.

[10] Xue W, Kong L, Zhang X, Xin Z, Zhao Q, He J, Wu W and Duan G. Tumor blood vessel in 3D reconstruction CT imaging as an risk indicator for growth of pulmonary nodule with ground-glass opacity. J Cardiothorac Surg 2023; 18: 333.

[11] Liu QX, Zhou D, Han TC, Lu X, Hou B, Li MY, Yang GX, Li QY, Pei ZH, Hong YY, Zhang YX, Chen WZ, Zheng H, He J and Dai JG. A noninvasive multianalytical approach for lung cancer diagnosis of patients with pulmonary nodules. Adv Sci (Weinh) 2021; 8: 2100104.

[12] Nam BD, Kim TJ, Lee KS, Kim TS, Han J and Chung MJ. Pulmonary mucormycosis: serial morphologic changes on computed tomography correlate with clinical and pathologic findings. Eur Radiol 2018; 28: 788-795.

[13] Panchabhai TS, Farver C and Highland KB. Lymphocytic interstitial pneumonia. Clin Chest Med 2016; 37: 463-474.

[14] El Alam R, Byrne SC and Hammer MM. Rate of benign nodule resection in a lung cancer screening program. Clin Imaging 2023; 104: 109984.

[15] Jiang H, Ma L, Qi XW, Yan LZ, Feng HX, Suo LJ and Liu B. Pulmonary benign metastasizing leiomyoma: a case report and literature review. Ann Palliat Med 2021; 10: 5831-5838.

[16] Gould MK, Tang T, Liu IL, Lee J, Zheng C, Danforth KN, Kosco AE, Di Fiore JL and Suh DE. Recent trends in the Identification of incidental pulmonary nodules. Am J Respir Crit Care Med 2015; 192: 1208-1214.

[17] Heerink WJ, de Bock GH, de Jonge GJ, Groen HJ, Vliegenthart R and Oudkerk M. Complication rates of CT-guided transthoracic lung biopsy: meta-analysis. Eur Radiol 2017; 27: 138-148.

[18] Goud A, Dahagam C, Breen DP and Sarkar S. Role of electromagnetic navigational bronchoscopy in pulmonary nodule management. J Thorac Dis 2016; 8 Suppl 6: S501-S508.

[19] Gong L, Jiang S, Yang Z, Zhang G and Wang L. Automated pulmonary nodule detection in CT images using 3D deep squeeze-and-excitation networks. Int J Comput Assist Radiol Surg 2019; 14: 1969-1979.
[20] Cao K, Meng G, Wang Z, Liu Y, Liu H and Sun L. An adaptive pulmonary nodule detection algorithm. J Xray Sci Technol 2020; 28: 427-447.
[21] Camidge DR, Mandair D, Morgan R, Amini A and Rusthoven CG. Quantifying the medical impact of a missed diagnosis of non-small cell lung cancer on chest imaging. Clin Lung Cancer 2022; 23: 377-385.
[22] Yang D, Du J, Liu K, Sui Y, Wang J and Gai X. Construction of U-Net++ pulmonary nodule intelligent analysis model based on feature weighted aggregation. Technol Health Care 2023; 31: 477-486.
[23] Choi MJ and Kang H. CT findings of central airway lesions causing airway stenosis-visualization and quantification: a pictorial essay. Taehan Yongsang Uihakhoe Chi 2021; 82: 1441-1476.
[24] Rikhari H, Baidya Kayal E, Ganguly S, Sasi A, Sharma S, Dheeksha DS, Saini M, Rangarajan K, Bakhshi S, Kandasamy D and Mehndiratta A. Fully automatic deep learning-based lung parenchyma segmentation and boundary correction in thoracic CT scans. Int J Comput Assist Radiol Surg 2024; 19: 261-272.
[25] Rivera GA and Wakelee H. Lung cancer in never smokers. Adv Exp Med Biol 2016; 893: 43-57.
[26] Thandra KC, Barsouk A, Saginala K, Aluru JS and Barsouk A. Epidemiology of lung cancer. Contemp Oncol (Pozn) 2021; 25: 45-52.
[27] Zhong M, Zhang Y, Pan Z, Wang W, Zhang Y, Weng Y, Huang H, He Y and Liu O. Clinical utility of circulating tumor cells in the early detection of lung cancer in patients with a solitary pulmonary nodule. Technol Cancer Res Treat 2021; 20: 15330338211041465.
[28] Zhou Q, He Q, Peng L, Huang Y, Li K, Liu K, Li D, Zhao J, Sun K, Li A and He W. Preoperative diagnosis of solitary pulmonary nodules with a novel hematological index model based on circulating tumor cells. Front Oncol 2023; 13: 1150539.